

Figure 8.1
Aircraft as a point mass.

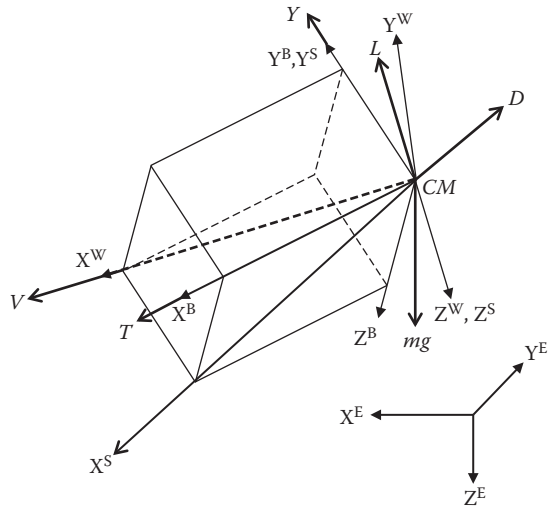


Figure 8.2

Forces acting on the aircraft (mg along Z^E , L along $-Z^W$, D along $-X^S$, Y along Y^B , T along X^B).

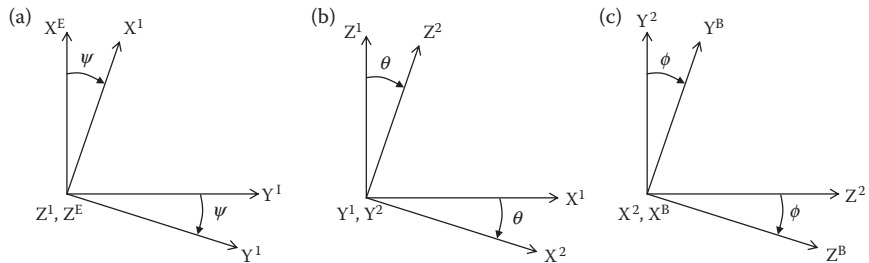


Figure 8.3

(a) Rotation '3' about the Z^E axis, (b) rotation '2' about Y^1 axis, (c) rotation '1' about X^2 axis.

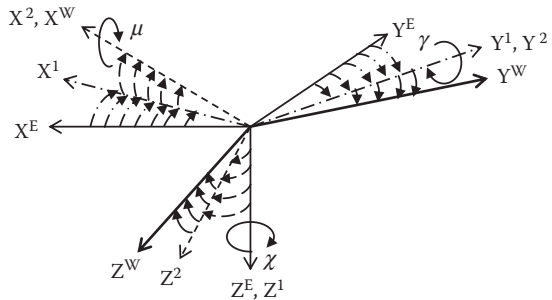


Figure 8.4
Rotations χ (about Z^E), γ (about Y^1) and μ (about X^2).

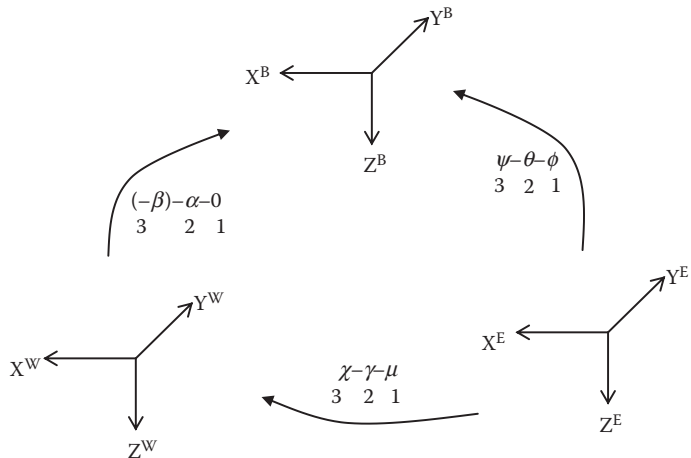


Figure 8.5
Schematic summary of rotations with sequence involved between the three coordinate systems used in flight dynamics.

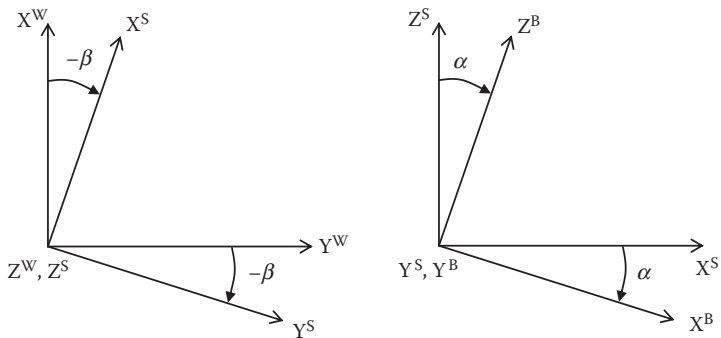


Figure 8.6
Rotations ($-\beta$) of wind axis system and α of the stability axis system.

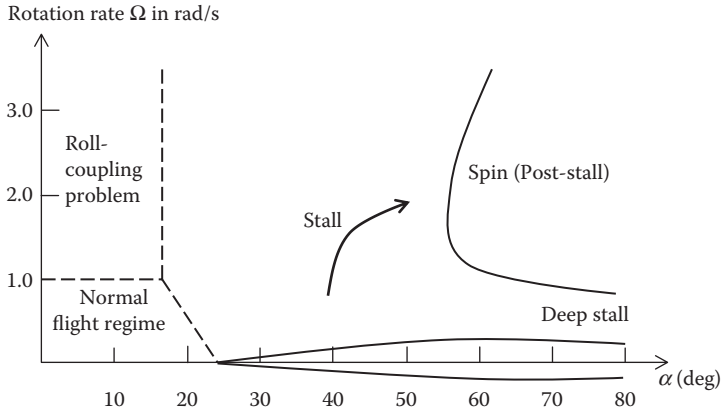


Figure 8.7

Flight regimes of aircraft. (Reprinted from Goman, M.G., Zagaynov, G.I. and Khrantsovsky, A.V., Application of bifurcation methods to nonlinear flight dynamics problems, *Progress in Aerospace Sciences*, Vol. 33, 1997, pp. 539–586. © 1997. With Permission from Elsevier.)

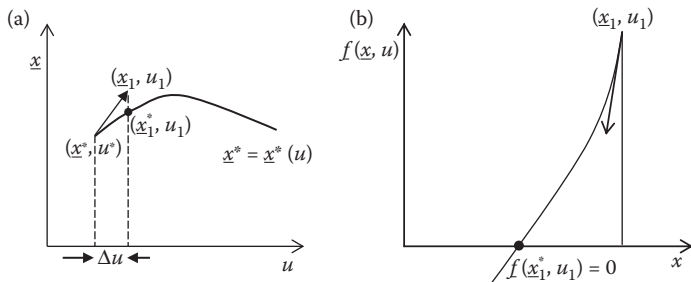


Figure 8.8

(a) Predictor step and (b) corrector step in a continuation.

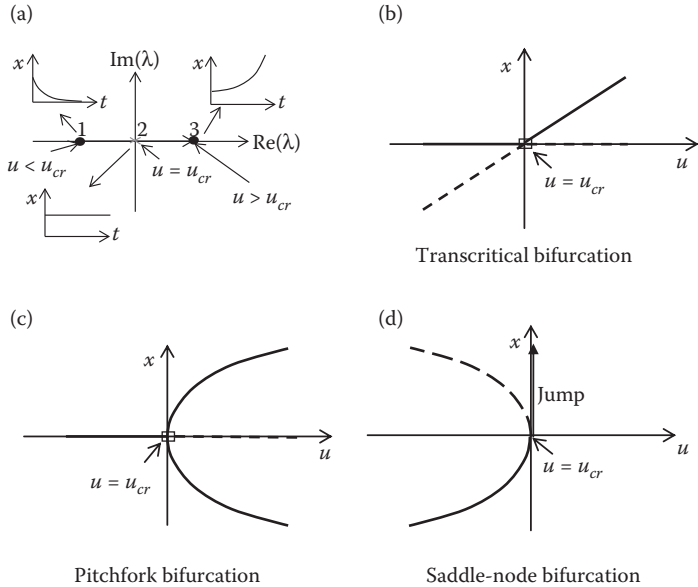


Figure 8.9
 Branch of stable (solid line) and unstable (dashed line) equilibrium states as functions of varying system parameter u . Disturbance time history is also plotted for three different locations of eigenvalues.

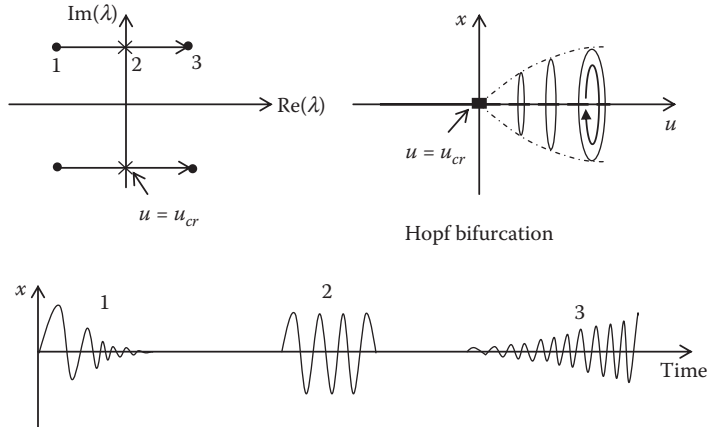


Figure 8.10

A pair of complex-conjugate eigenvalues crossing imaginary axis leading to bifurcation from stable equilibrium state to stable oscillatory state at $u = u_{cr}$. Time simulation results corresponding to three locations of eigenvalues are also shown.

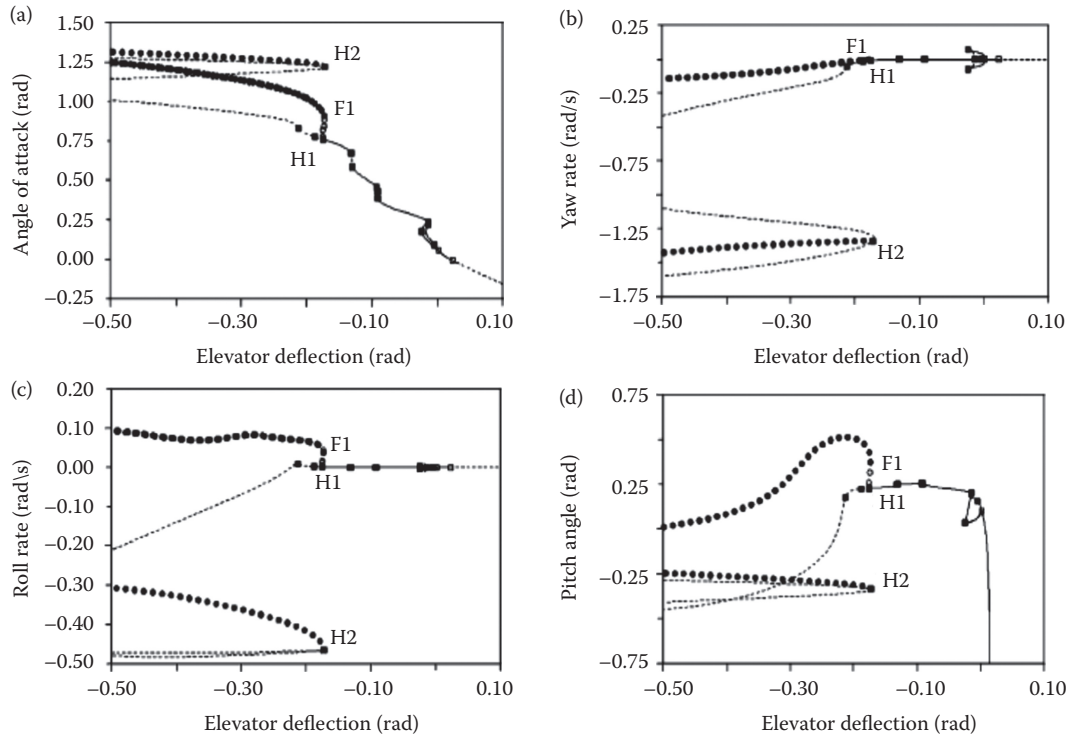


Figure 8.11

Bifurcation plots of the F-18/HARV model as function of the elevator deflection (solid line: stable trim, dashed line: unstable trim, solid circle: stable oscillatory state, empty circle: unstable oscillatory state, empty square: pitchfork bifurcation, solid square: Hopf bifurcation).

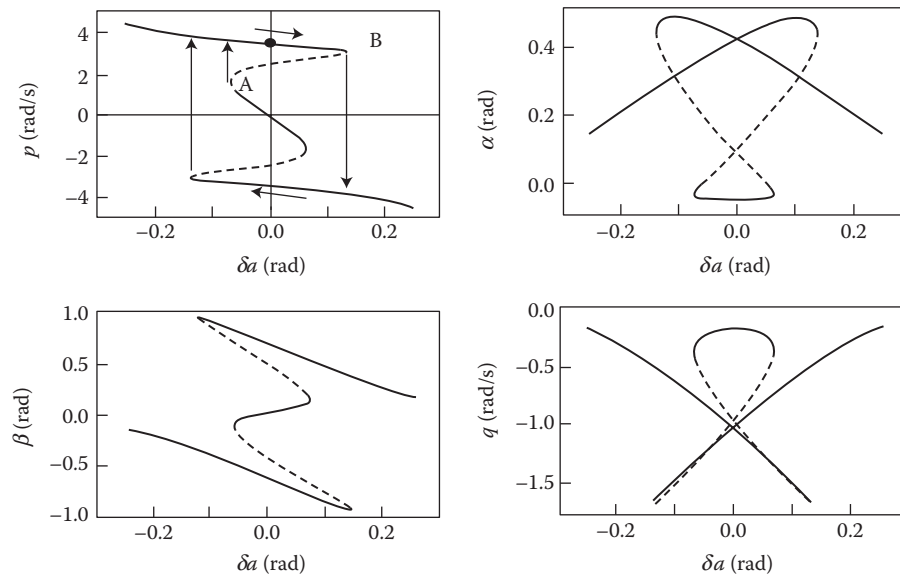


Figure 8.12
 PSS roll rate and other variables as a function of aileron deflection δa , with $\delta e = -2^\circ$, $\delta r = 0$ (solid lines: stable states; dashed lines: unstable states).

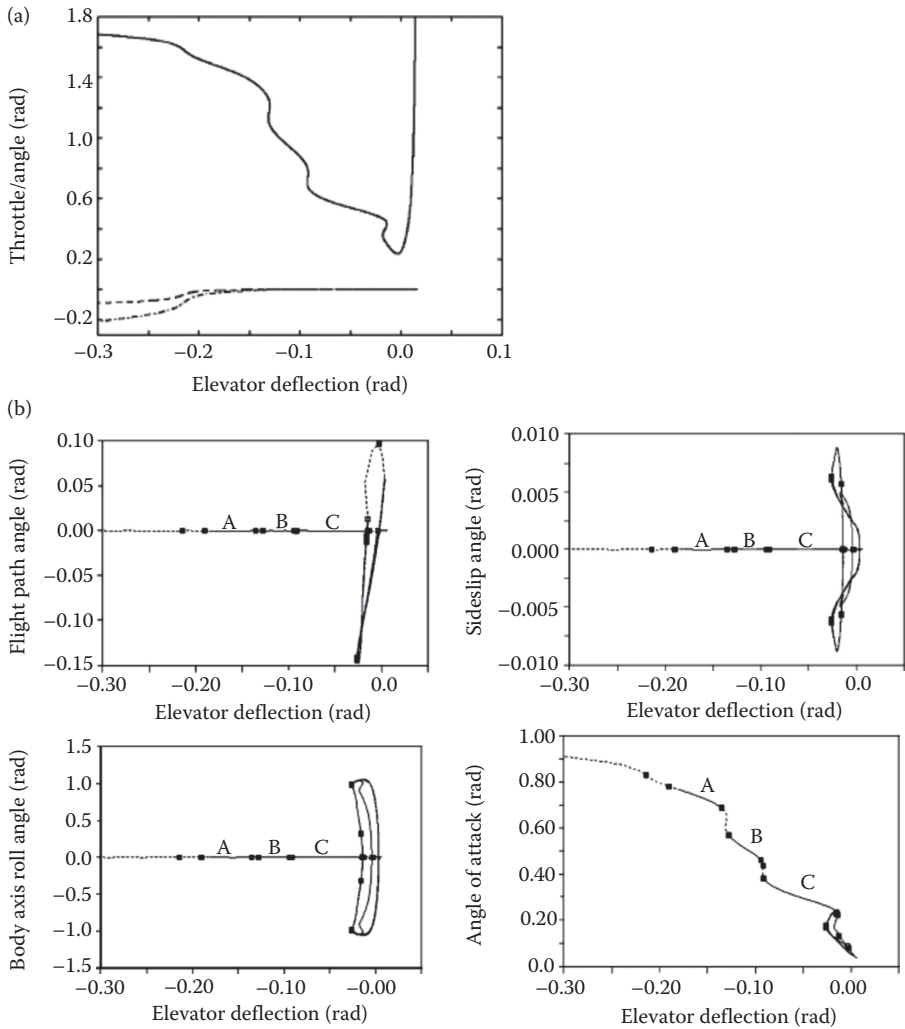


Figure 8.13
 (a) Thrust fraction (full line), aileron (dash-dot line), rudder (dashed line) versus elevator deflection schedule and (b) Bifurcation plots of Straight and level flight trim states as function of elevator deflection (solid lines: stable trims, dashed lines: unstable trims, empty squares: pitchfork bifurcations, solid squares: Hopf bifurcation).

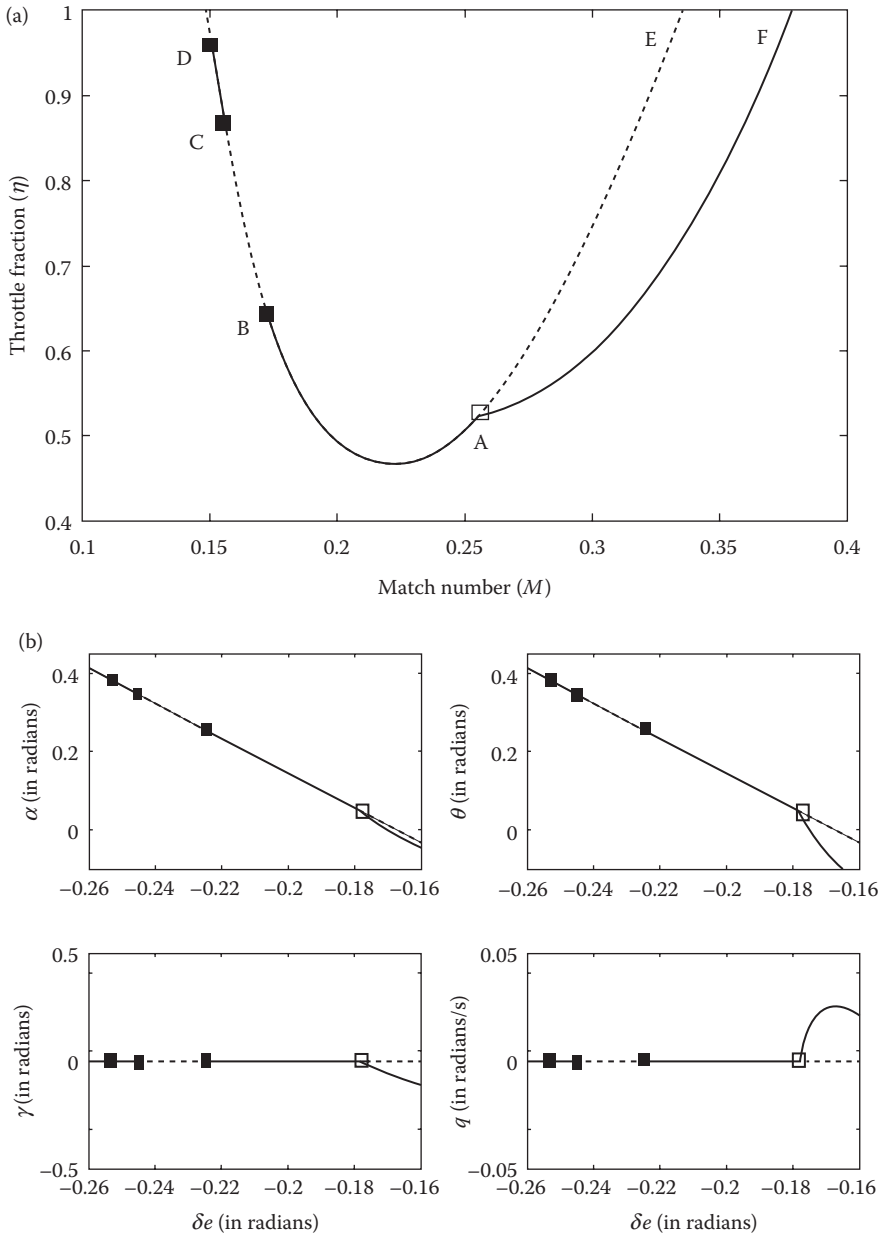


Figure 8.14 Bifurcation diagram of (a) throttle fraction in straight and level flight trim condition as a function of the Mach number, (b) and (c) other variables as functions of elevator deflection (solid lines: stable trims; dashed lines: unstable trims; empty squares: pitchfork bifurcations; solid squares: Hopf bifurcation) and (d) root locus plot with variation in trim angle of attack.

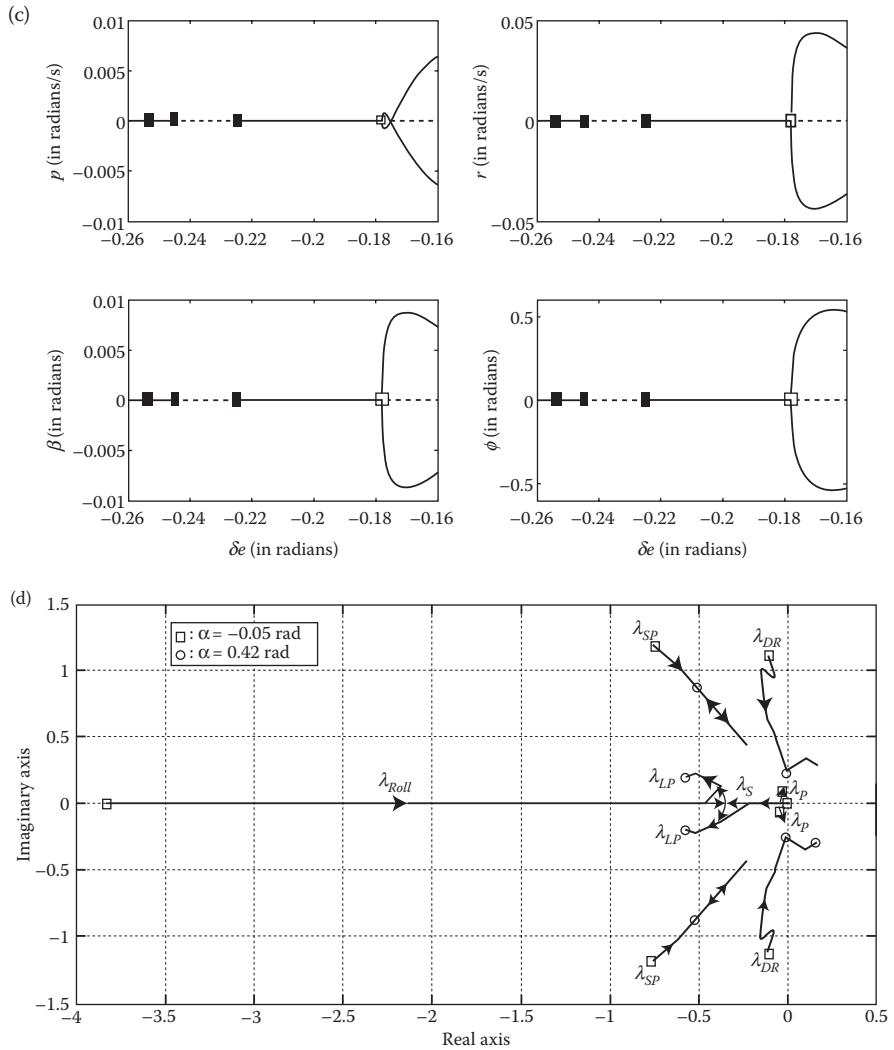


Figure 8.14 (continued)

Bifurcation diagram of (a) throttle fraction in straight and level flight trim condition as a function of the Mach number, (b) and (c) other variables as functions of elevator deflection (solid lines: stable trims; dashed lines: unstable trims; empty squares: pitchfork bifurcations; solid squares: Hopf bifurcation) and (d) root locus plot with variation in trim angle of attack.

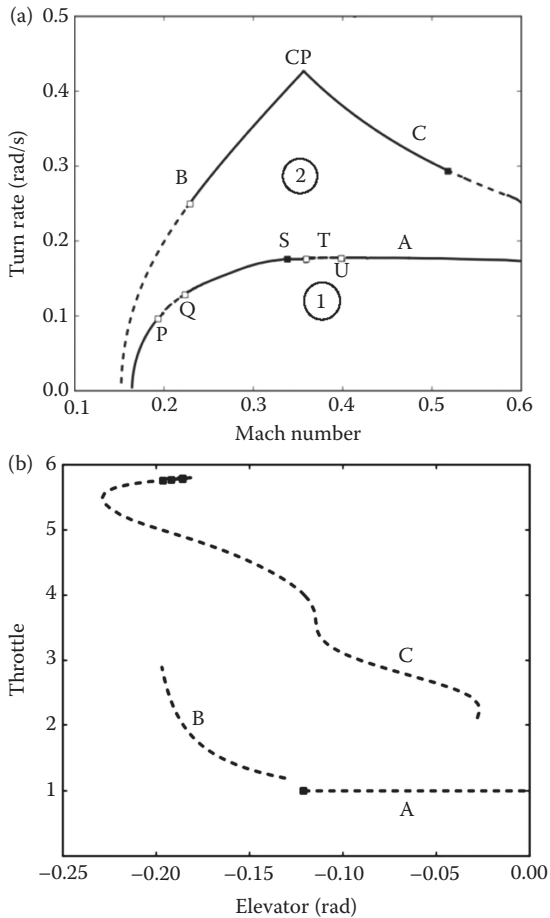


Figure 8.15

Bifurcation plots of level turn flight trim states as a function of the Mach number (solid lines: stable trims; dashed lines: unstable trims; empty squares: pitchfork bifurcations; solid squares: Hopf bifurcation).

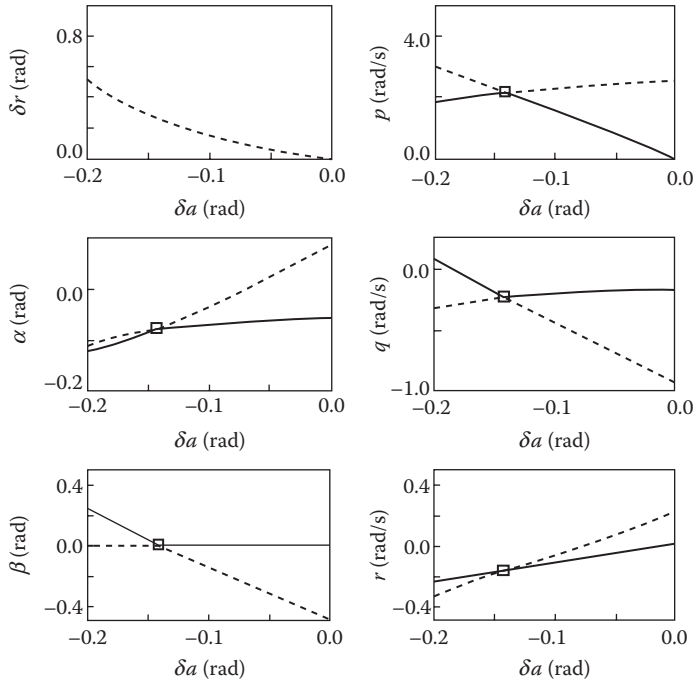


Figure 8.16

Zero sideslip aileron–rudder interconnect (ARI) law (top left) and corresponding PSS solutions (solid lines: stable solutions; dashed lines: unstable solutions; empty square: transcritical bifurcation).

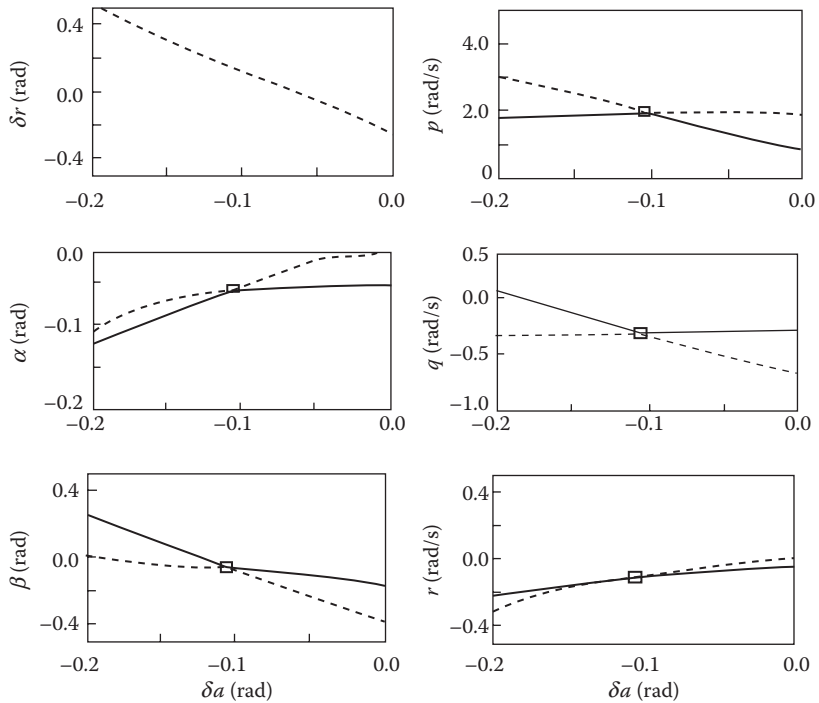


Figure 8.17

Velocity-vector roll aileron-rudder interconnect (ARI) law (top left) and corresponding PSS solutions (solid lines: stable solutions; dashed lines: unstable solutions; empty square: transcritical bifurcation).